

# Functionalized UiO-66 by Single and Binary $(\text{OH})_2$ and $\text{NO}_2$ Groups for Uptake of $\text{CO}_2$ and $\text{CH}_4$

Zana Hassan Rada,<sup>†</sup> Hussein Rasool Abid,<sup>†,‡</sup> Jin Shang,<sup>§</sup> Hongqi Sun,<sup>†</sup> Yingdian He,<sup>§</sup> Paul Webley,<sup>§</sup> Shaomin Liu,<sup>†</sup> and Shaobin Wang<sup>\*,†</sup>

<sup>†</sup>Department of Chemical Engineering, Curtin University, GPO Box U1987, Perth Western Australia 6845, Australia

<sup>‡</sup>Department of Environmental Health, Applied Medical Science College, Karbala University, Karbala, Iraq

<sup>§</sup>Department of Chemical and Biomolecular Engineering, The University of Melbourne, Parkville, Victoria 3010, Australia

**ABSTRACT:** The metal–organic frameworks UiO-66 with single or binary  $-(\text{OH})_2$  and  $-\text{NO}_2$  functional groups were synthesized, and their structures and properties were characterized by Fourier transform infrared spectroscopy, X-ray diffraction, thermogravimetric analysis, scanning electron microscopy, and nitrogen adsorption isotherms. Their performances in  $\text{CO}_2$  and  $\text{CH}_4$  adsorption at high pressures and different temperatures (273 and 298 K) were also determined. Singly functionalized UiO-66-(OH)<sub>2</sub> had a lower thermal stability than UiO-66-NO<sub>2</sub>, but the thermal stability of binary UiO-66-(OH)<sub>2</sub>-NO<sub>2</sub> significantly improved to 650 K. The binary-functionalized samples UiO-66-(OH)<sub>2</sub>-NO<sub>2</sub> and UiO-66-NO<sub>2</sub>-(OH)<sub>2</sub> displayed higher  $\text{CH}_4$  and  $\text{CO}_2$  adsorption than UiO-66-(OH)<sub>2</sub> and UiO-66-NO<sub>2</sub>. The  $\text{CO}_2$  adsorption capacities of UiO-66-(OH)<sub>2</sub>-NO<sub>2</sub> and UiO-66-NO<sub>2</sub>-(OH)<sub>2</sub> were 4.65 and 7.35 mmol/g, respectively, at 273 K and 900 kPa. UiO-66-(OH)<sub>2</sub> had a higher separation factor for selective separation of  $\text{CO}_2$  from  $\text{CH}_4$ , especially at low pressures up to 100 kPa; the separation factor ranged from 4.9 at about 100 kPa to 5.8 at 60 kPa.

## 1. INTRODUCTION

Metal–organic frameworks (MOFs) are a new class of crystalline and porous materials that can be shaped in 1D, 2D, and 3D networks through coordination bonds between metal clusters or metal ions and organic ligands (linkers).<sup>1–3</sup> The different metal and linker connections can generate MOFs with many characteristics such as high specific surface area, high pore volume, and low density. In addition, the varying textural properties of MOFs lead them to be widely used in many applications, for instance, adsorption and storage of gases such as  $\text{CO}_2$ ,  $\text{CH}_4$ , and  $\text{H}_2$ , separation and catalysis,<sup>4–7</sup> and drug delivery.<sup>8</sup>

$\text{CO}_2$  emissions into the atmosphere and its concentration have increased in the past century; the emissions are almost 6 billion tons per year, and the  $\text{CO}_2$  concentration in the atmosphere has risen to 400 ppm since the start of the industrial era. The increase in carbon dioxide emissions mostly results from human activities during rapid industrial development,<sup>9,10</sup> causing a global climate change. Nevertheless, one of solutions to reduce the  $\text{CO}_2$  contribution to the climate change is separation of  $\text{CO}_2$  from flue gases and sequestration, which can be achieved by a number of technologies, for example, adsorption. Thus, adsorptive separation processes using MOFs as adsorbents have attracted attention from many researchers in regard to increasing the adsorption capacities and enhancing the specific selectivities for various gases such as  $\text{CO}_2$ ,  $\text{CH}_4$ , and  $\text{N}_2$ .<sup>11,12</sup> For example, the enhancement of  $\text{CO}_2/\text{N}_2$  and  $\text{CO}_2/\text{CH}_4$  selectivity via Zn-based MOFs has been reported by Bae and co-workers.<sup>13,14</sup>

The enhancement of  $\text{CO}_2$  and  $\text{CH}_4$  adsorption capacities on MOFs can be achieved by improving the structural design and properties of MOFs through several strategies,<sup>15</sup> such as pore size control,<sup>16</sup> open metal sites,<sup>17</sup> and polar functional groups.<sup>18,19</sup>

A polar functional group modification can be achieved by two approaches, direct assembly and postsynthesis, and these approaches can also change the MOF properties such as the pore size and surface area.<sup>15</sup> Several polar functional groups ( $-\text{NH}_2$ ,  $-\text{NO}_2$ ,  $-\text{OH}$ , etc.) have been used to prepare functionalized MOFs to enhance the uptake of  $\text{CO}_2$  and  $\text{CH}_4$ .<sup>20–22</sup>

Zr-based MOFs (UiO-66)<sup>23</sup> have attracted the attention of researchers and have been modified in direct synthesis using different functionalized linkers for adsorption and separation of  $\text{CO}_2$  and  $\text{CH}_4$ .<sup>24,25</sup> Recently, mixed-functional-group-based MOFs (MixMOFs) have been studied for  $\text{CO}_2$  and  $\text{CH}_4$  adsorption.<sup>26</sup> However, few MixMOFs from UiO-66 have been investigated. The mixed linkers 2,5-bromo-1,3-benzenedicarboxylate (BDC-Br, nonpolar) and 2-aminoterephthalic acid (BDC-NH<sub>2</sub>, polar) have been used to synthesize bifunctionalized UiO-66-Br<sub>2</sub>-NH<sub>2</sub>,<sup>27</sup> and the nonfunctionalized linker 1,4-benzenedicarboxylate (BDC) mixed with BDC-NH<sub>2</sub> has also been used for the synthesis of UiO-66.<sup>28</sup> In this work, two polar functionalized linkers, BDC-(OH)<sub>2</sub> and BDC-NO<sub>2</sub>, were employed to prepare MixMOFs of UiO-66, and the samples were characterized and compared with singly functionalized UiO-66-(OH)<sub>2</sub> and UiO-66-NO<sub>2</sub> in regard to textural properties and  $\text{CO}_2$  and  $\text{CH}_4$  adsorption.

**Special Issue:** International Conference on Carbon Dioxide Utilization 2015

**Received:** October 28, 2015

**Revised:** December 16, 2015

**Accepted:** December 16, 2015

## 2. EXPERIMENTAL SECTION

**2.1. Chemicals.** Zirconium chloride ( $ZrCl_4$ , 99.9%), 2-nitrotetraphthalic acid ( $BDC\text{-NO}_2$ , ≥99%), 2,5-dihydroxybenzenediacrylic acid ( $BDC\text{-(OH)}_2$ ), *N,N*-dimethylformamide (DMF,  $C_3H_7NO$ , 98%), methanol ( $CH_3OH$ , 99%), acetic acid (>80% by mass), and ethanol (absolute, >99%) were supplied by Sigma-Aldrich, Scientific Perth, and Thermo Fisher Scientific without further purification.

**2.2. Synthesis.** A new solvothermal procedure was used to prepare  $\text{UiO-66-(OH)}_2$  and  $\text{UiO-66-(OH)}_2\text{-NO}_2$ . This method is different from the one for Zr-based MOFs.  $\text{UiO-66-NO}_2$  and  $\text{UiO-66-NO}_2\text{-(OH)}_2$  were synthesized as in our previous study.<sup>29</sup>

$\text{UiO-66-(OH)}_2$  was synthesized by dissolving 5.15 mmol of  $ZrCl_4$  and 2.63 mmol of  $BDC\text{-(OH)}_2$  in 774.93 mmol of DMF. After 15 min of mixing, 349.3 mmol of acetic acid and 171.26 mmol of ethanol were added to the mixture during the mixing. Then the produced solution was placed in a 125 mL autoclave, which was sealed and heated in an oven preheated to 403 K for 2 days. Finally, a yellow crystalline sample was extracted under vacuum from the solution.

$\text{UiO-66-(OH)}_2\text{-NO}_2$  was obtained using a similar procedure with some modifications. First, 2.65 mmol of  $BDC\text{-(OH)}_2$  was mixed with 0.265 mmol of  $BDC\text{-NO}_2$  and 5.2 mmol of  $ZrCl_4$  in 86 mL of DMF for 40 min. After that, 349.3 mmol of acetic acid and 171.26 mmol of ethanol were added to the mixture for 15 min, and then the homogeneous mixture was placed in a Parr PTFE-lined digestion vessel with a volume of 125 mL. The digestion vessel was placed in an oven preheated to 393 K for 24 h, after which the autoclave was cooled to room temperature and a yellow crystalline product was obtained by vacuum filtration.

**2.3. Activation.** All of the samples were activated using the previously reported method.<sup>30,31</sup> For each activation, a 0.3 g sample was immersed in a methanol solution for 3 days. After that, the sample was filtered and dried at 373 K, and then all of the solid materials were heated under vacuum at 453 K for 2 days.

**2.4. Characterization of Samples.** Powder X-ray diffraction (XRD) patterns were obtained on an X-ray diffractometer (D8 Advance, Bruker AXS) in transmission mode using  $Cu K\alpha$  radiation ( $\lambda = 1.5406 \text{ \AA}$ ), a low angle range of  $2\theta = 5\text{--}70^\circ$ , a voltage of 40 kV, and a current of 40 mA to determine the crystalline structures of the samples. The intensities of

functional groups on all of the samples were determined using an FTIR spectrometer (100 FT-IR, PerkinElmer). The spectrum was scanned from 600 to 4000  $\text{cm}^{-1}$  with a resolution of 4  $\text{cm}^{-1}$  using the attenuated total reflectance (ATR) technique. The thermal stabilities of the samples were determined by thermogravimetric analysis (TGA) using a TGA/DSC1 STAR<sup>e</sup> system (Mettler-Toledo). A sample of 8–20 mg was loaded into a 150  $\mu\text{L}$  alumina pan and placed automatically in the TGA furnace to be heated in an atmosphere consisting of an Ar/air gas mixture at a rate of 10 K/min from lab temperature up to 1373 K. The morphologies of the samples were obtained by scanning electron microscopy (SEM) on a NEON 40 EsB Cross-Beam scanning electron microscope (Zeiss). A Tristar 3000 analyzer (Micromeritics) was used to determine the surface areas and pore sizes of samples using the Brunauer–Emmett–Teller (BET) and Barrett–Joyner–Halenda (BJH) methods, respectively, by measurement of  $N_2$  adsorption/desorption isotherms at 77 K.

**2.5. Adsorption Measurements.** Adsorption isotherms of pure  $\text{CO}_2$  and  $\text{CH}_4$  on the samples at pressures up to 1000 kPa were evaluated using an ASAP2050 analyzer (Micromeritics). First of all, 0.2 g of sample was degassed on the ASAP2050 instrument by stepwise heating at 1 K/min up to 453 K and holding at this temperature for 8 h under high vacuum. Carbon dioxide (99.995%) and methane (99.995%) were supplied by Coregas.

## 3. RESULTS AND DISCUSSION

The XRD patterns in Figure 1 indicate that the structures of Zr-MOFs with single or binary functional groups are similar to that of  $\text{UiO-66}$  as previously reported.<sup>23,31</sup> It was also observed that the reflections of  $\text{UiO-66-(OH)}_2$  were reduced a bit and were weaker than those of  $\text{UiO-66-NO}_2\text{-(OH)}_2$  and  $\text{UiO-66-NO}_2$ . This may be attributed to reduced crystal size of  $\text{UiO-66-(OH)}_2$  or to reduced crystallinity.

Figure 2 displays TGA and DTG profiles for all of the samples. It can be seen that  $\text{UiO-66-NO}_2$  was thermally stable until 670 K. After 670 K, the interconnection of  $\text{NO}_2$  groups between the free  $BDC\text{-NO}_2$  molecules and the nitro functional groups of the coordinated organic linkers inside the pores were broken, and the structure collapsed to produce  $ZrO_2$ . It can also be observed that more than 98% of free and coordinated solvent molecules (DMF) were removed in the activation process

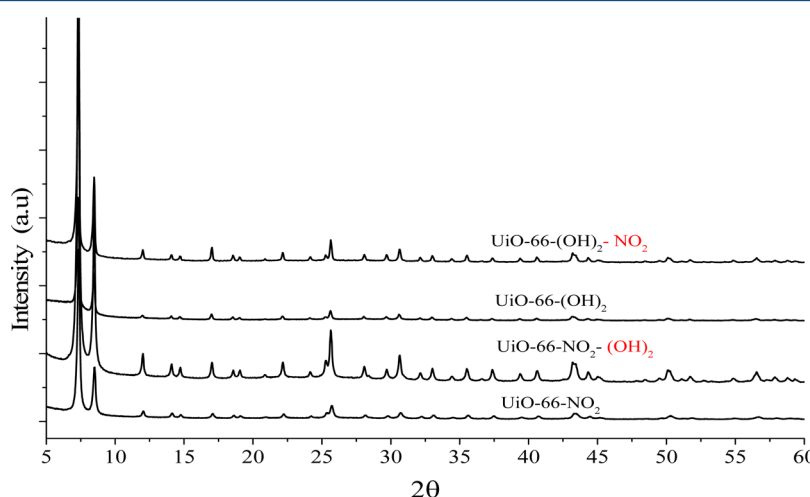
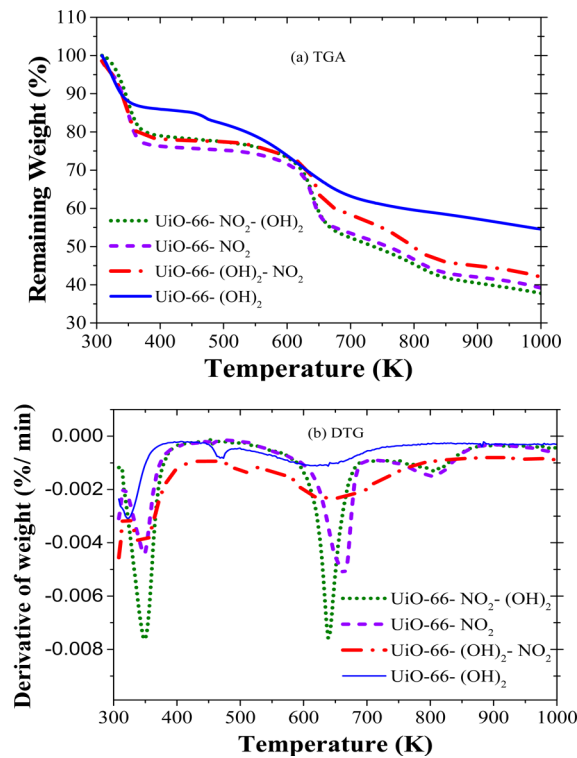


Figure 1. XRD patterns of  $\text{UiO-66}$  samples.



**Figure 2.** TGA and DTG profiles of various  $\text{UiO-66}$  samples.

and that little weight loss occurred at temperatures of 400–600 K. However, loading of the  $\text{BDC}-(\text{OH})_2$  functional group on the  $\text{UiO-66-NO}_2$  sample reduced the thermal stability to 640 K, and more details can be found in our previous study.<sup>29</sup> The structure of  $\text{UiO-66-(OH)}_2$  started to decompose at around 480 K, earlier than  $\text{UiO-66-NO}_2$ , as a result of the higher polarity of hydroxyl functional groups compared with  $\text{NO}_2$  groups. The gradual thermal decomposition curve of  $\text{UiO-66-(OH)}_2$  also suggests no homogeneity in the bonding of interconnection. Thermal analysis also showed that  $\text{UiO-66-(OH)}_2\text{-NO}_2$  sample was thermally stable up to 650 K, which is higher than for  $\text{UiO-66-(OH)}_2$  sample. This may be due to loading of the  $\text{BDC-NO}_2$  group for improved interconnection.

Figure 3 describes the possible functional groups in the structures of  $\text{UiO-66-(OH)}_2$ ,  $\text{UiO-66-(OH)}_2\text{-NO}_2$ ,  $\text{UiO-66-NO}_2$ , and  $\text{UiO-66-NO}_2\text{-(OH)}_2$ . The free carboxylic functional group ( $\text{O=COH}$ ) can be seen by the peak at  $1650 \text{ cm}^{-1}$  for nonactivated samples, while no such peak can be found for the activated samples because the group was removed by methanol activation. The hydroxyl group was observed by the peak at  $3300 \text{ cm}^{-1}$  on  $\text{UiO-66-(OH)}_2$ ,  $\text{UiO-66-(OH)}_2\text{-NO}_2$ , and  $\text{UiO-66-NO}_2\text{-(OH)}_2$  in the activated and nonactivated samples. The bands at  $1430\text{--}1533 \text{ cm}^{-1}$  occurred in the spectra of all of the samples, indicating the presence of hydroxyl groups in the coordinated linkers. In addition, it can be seen that the strongest peak is at  $1240 \text{ cm}^{-1}$ , relating to C–O stretching of OH functional groups on benzene rings. Furthermore, it can be observed that 2,5-hydroxy-1,4-benzenedicarboxylate was coordinated to the zirconium metal center by the  $-\text{CO}_2$  asymmetric ( $1500$  and  $1597 \text{ cm}^{-1}$ ) and symmetric stretching peaks ( $1340$  and  $1456 \text{ cm}^{-1}$ ). The peak at  $772 \text{ cm}^{-1}$  refers to bending of the C–H functional groups on benzene rings at mono or ortho positions. For  $\text{UiO-66-NO}_2$  and  $\text{UiO-66-NO}_2\text{-(OH)}_2$  samples, the aromatic carboxylate salt with the nitro functional group can be recognized by the peak at  $1536 \text{ cm}^{-1}$ . The  $-\text{CO}_2$

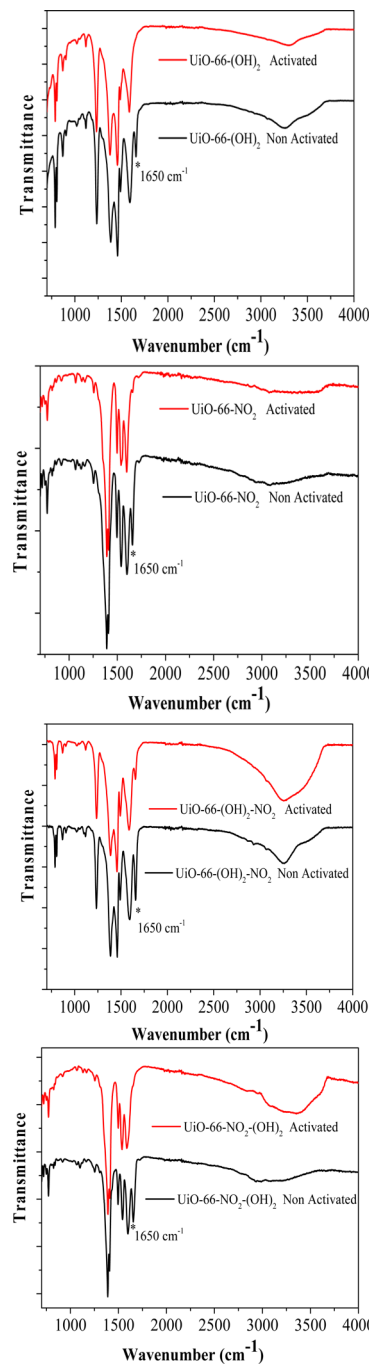


**Figure 3.** FTIR spectra of functionalized  $\text{UiO-66}$  samples before and after activation.

groups coordinated to the metal centers were shown by the asymmetric ( $1590$  and  $1495 \text{ cm}^{-1}$ ) and symmetric ( $1409$  and  $1389 \text{ cm}^{-1}$ ) stretching peaks.

Figure 4 shows that the nitrogen adsorption/desorption isotherms for the  $\text{UiO-66-(OH)}_2$ ,  $\text{UiO-66-(OH)}_2\text{-NO}_2$ ,  $\text{UiO-66-NO}_2$ , and  $\text{UiO-66-NO}_2\text{-(OH)}_2$  samples have obvious differences in micropores and hysteresis loops.  $\text{UiO-66-(OH)}_2$  and  $\text{UiO-66-(OH)}_2\text{-NO}_2$  exhibited larger hysteresis loops than  $\text{UiO-66-NO}_2$  and  $\text{UiO-66-NO}_2\text{-(OH)}_2$  because of the presence of mesopores. The existence of mesopores was accompanied by narrow cages in  $\text{UiO-66-(OH)}_2$  at relative pressures of  $0.4\text{--}0.9$ . The BET surface areas of singly functionalized  $\text{UiO-66-(OH)}_2$  and  $\text{UiO-66-NO}_2$  are  $396$  and  $771 \text{ m}^2/\text{g}$ , respectively, while the

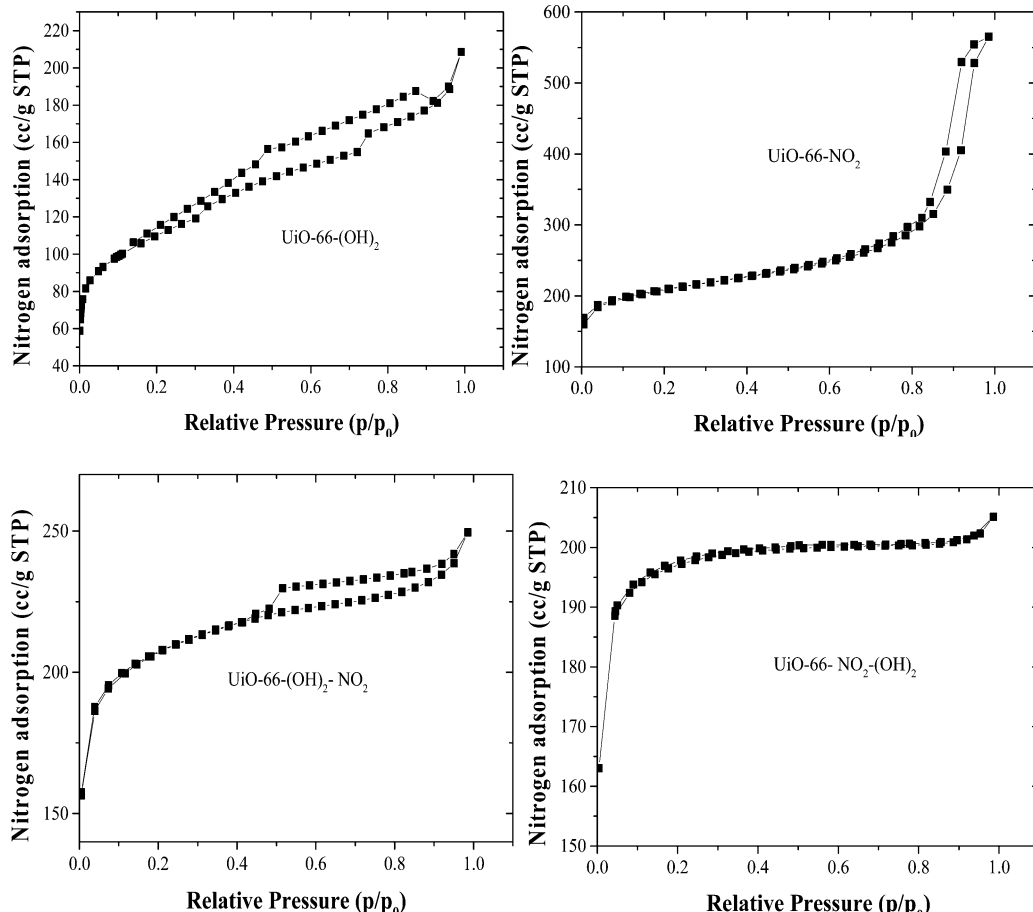


**Figure 4.** Nitrogen adsorption/desorption isotherms of various  $\text{UiO-66}$  samples.

**Table 1. Pore Structures of  $\text{UiO-66}$  Samples**

	$\text{UiO-66-(OH)}_2$	$\text{UiO-66-(OH)}_2\text{-NO}_2$	$\text{UiO-66-NO}_2$	$\text{UiO-66-NO}_2\text{-(OH)}_2$
$S_{\text{BET}}$ ( $\text{m}^2/\text{g}$ )	397	778	771	732
$V_{\text{micropore}}$ ( $\text{cm}^3/\text{g}$ )	0.17	0.24	0.21	0.27

binary-functionalized  $\text{UiO-66-(OH)}_2\text{-NO}_2$  and  $\text{UiO-66-NO}_2\text{-(OH)}_2$  samples show BET surface areas of 778 and 732  $\text{m}^2/\text{g}$ , respectively. It seems that the BET surface area of binary-functionalized  $\text{UiO-66-(OH)}_2\text{-NO}_2$  is significantly increased by loading with a  $\text{NO}_2$  group, while adding  $(\text{OH})_2$  groups to  $\text{UiO-66-NO}_2$  slightly decreases the surface area of binary-functionalized  $\text{UiO-66-NO}_2\text{-(OH)}_2$ .<sup>29</sup> As a result of the high polarity of the hydroxyl functional groups and their strong interactions with metal ions and solvents, removal of the linker molecules ( $\text{BDC-(OH)}_2$ ) from the structure and the formation of pores will be retarded, resulting in a much lower surface area of  $\text{UiO-66-(OH)}_2$ . Similarly, addition of  $\text{BDC-(OH)}_2$  could also induce a lower surface area of  $\text{UiO-66-NO}_2\text{-(OH)}_2$  compared with  $\text{UiO-66-NO}_2$ . The micropore volumes of  $\text{UiO-66-(OH)}_2$ ,  $\text{UiO-66-(OH)}_2\text{-NO}_2$ ,  $\text{UiO-66-NO}_2$ , and  $\text{UiO-66-NO}_2\text{-(OH)}_2$  samples are 0.17, 0.24, 0.21, and 0.27  $\text{cm}^3/\text{g}$ , respectively (Table 1), demonstrating the enhancement of the micropore volume by the addition of polar groups.

SEM images of  $\text{UiO-66-(OH)}_2$  and  $\text{UiO-66-(OH)}_2\text{-NO}_2$  are shown in Figure 5. The morphology of  $\text{UiO-66-NO}_2$  and  $\text{UiO-66-NO}_2\text{-(OH)}_2$  particles was determined to be a triangular-base pyramid shape with a size of about 200 nm, as reported in a previous study.<sup>29</sup> For  $\text{UiO-66-(OH)}_2$  and  $\text{UiO-66-(OH)}_2\text{-NO}_2$ ,

homogeneous cubic particles were identified with a crystal size of about 100 nm, which is smaller than that of  $\text{UiO-66-NO}_2$  and  $\text{UiO-66-NO}_2\text{-(OH)}_2$ . The difference can be related to the use of multiple solvents, including ethanol, in the synthesis procedure for  $\text{UiO-66-(OH)}_2$  and  $\text{UiO-66-(OH)}_2\text{-NO}_2$ .

Figure 6 displays  $\text{CO}_2$  and  $\text{CH}_4$  adsorption isotherms on  $\text{UiO-66-(OH)}_2$ ,  $\text{UiO-66-(OH)}_2\text{-NO}_2$ ,  $\text{UiO-66-NO}_2$ , and  $\text{UiO-66-NO}_2\text{-(OH)}_2$  at 273 and 298 K.  $\text{UiO-66-(OH)}_2$  shows the adsorption of both  $\text{CO}_2$  and  $\text{CH}_4$  gases with capacities of 4.23 and 1.6 mmol/g, respectively, at 273 K and 900 kPa, while their adsorption capacities are 3.25 and 1.1 mmol/g, respectively, at 298 K and 900 kPa. Although  $\text{UiO-66-(OH)}_2$  has hydroxyl functional groups, which have higher polarity and greater affinity to adsorb carbon dioxide than the nitro functional groups, the adsorption uptakes by the  $\text{UiO-66-(OH)}_2$  sample are lower than those of the  $\text{UiO-66-(OH)}_2\text{-NO}_2$ ,  $\text{UiO-66-NO}_2$ , and  $\text{UiO-66-NO}_2\text{-(OH)}_2$  samples. The low adsorption capacity of  $\text{UiO-66-(OH)}_2$  is due to the strong chemical connections between the OH groups of the organic linkers and the metal cores. The structure of  $\text{UiO-66-(OH)}_2$  is similar to that of  $\text{UiO-66}$ , consisting of an inner  $\text{Zr}_6\text{O}_4(\text{OH})_4$  core in which the triangular faces of the  $\text{Zr}_6$  octahedron are alternatively capped by  $\mu_3\text{-O}$  and  $\mu_3\text{-OH}$  groups.<sup>23</sup> Also, another interaction

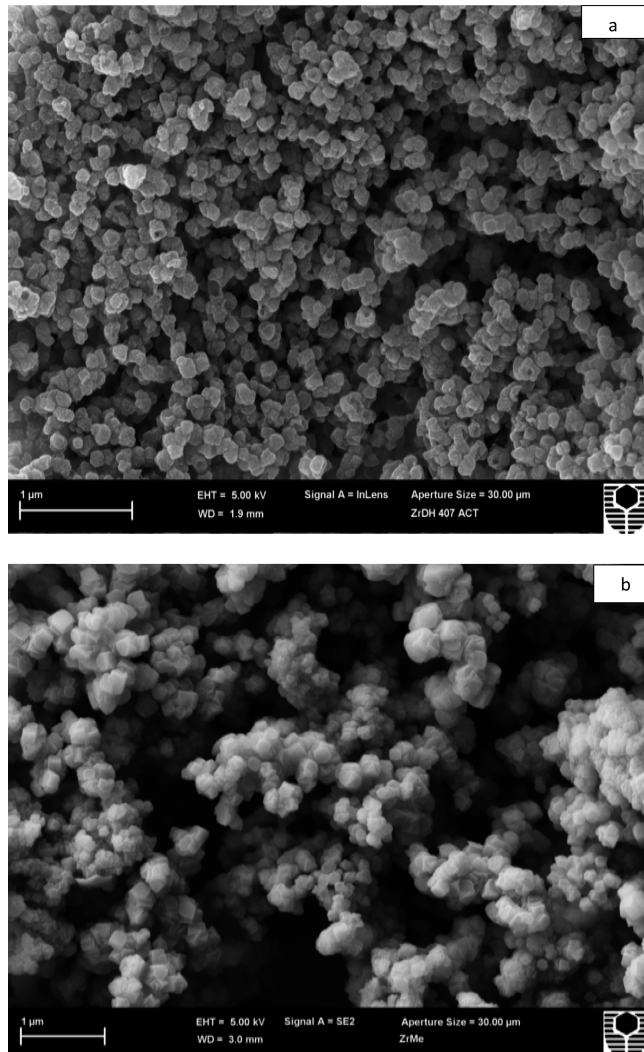


Figure 5. SEM images of (a)  $\text{UiO-66-(OH)}_2$  and (b)  $\text{UiO-66-(OH)}_2\text{-NO}_2$ .

occurs between the OH group of free  $\text{BDC-(OH)}_2$  and molecules of solvents (methanol, ethanol, or acetic acid) inside the pores. These bindings can cause a decrease in the surface area as well as the polarity of hydroxyl functional groups and the  $\text{CO}_2$  adsorption propensity. The  $\text{CO}_2$  adsorption capacity of the  $\text{UiO-66-NO}_2$  sample is higher than that of  $\text{UiO-66-(OH)}_2$  but lower than those of Zr-MOF ( $\text{UiO-66}$ )<sup>32</sup> and Zr-MOF-NH<sub>2</sub> ( $\text{UiO-66-NH}_2$ ).<sup>24</sup> The BET surface area of  $\text{UiO-66-NO}_2$  is lower, and the  $-\text{NO}_2$  functional groups in the  $\text{UiO-66-NO}_2$  structure cannot directly interact with  $\text{CO}_2$  for improved adsorption.

The MixMOF samples  $\text{UiO-66-(OH)}_2\text{-NO}_2$  and  $\text{UiO-66-NO}_2\text{-(OH)}_2$  showed an improvement in the adsorption capacities of  $\text{CO}_2$  and  $\text{CH}_4$  gases compared with the single-linker samples. The uptakes of  $\text{CO}_2$  and  $\text{CH}_4$  by the  $\text{UiO-66-(OH)}_2\text{-NO}_2$  sample increased to the values of 4.65 and 1.9 mmol/g at 273 K and 3.73 and 1.4 mmol/g at 298 K, respectively. This is the case because the  $-\text{NO}_2$  functional group may lead to an increase in the polarity of the organic linkers by changing the charge distribution, which may indirectly enhance the  $\text{CO}_2$  adsorption.<sup>33,34</sup> In the same way, by addition of the  $\text{BDC-(OH)}_2$  functional group into the  $\text{UiO-66-NO}_2$  sample, the uptakes of  $\text{CO}_2$  and  $\text{CH}_4$  were also improved,<sup>35</sup> showing the values of 7.35 and 3.4 mmol/g at 273 K and 5.73 and 2.4 mmol/g at 298 K, respectively. Moreover, it can be seen from Figure 6

that all of the samples have higher adsorption capacities for  $\text{CO}_2$  than for  $\text{CH}_4$  as a result of the fact that  $\text{CO}_2$  has a significant quadrupole moment ( $13.4 \times 10^{40} \text{ cm}^2$ ) and strongly interacts with adsorbents while  $\text{CH}_4$  has no quadrupole moment.<sup>36</sup> The micropores within the solid structure might also affect the ability of the samples to adsorb  $\text{CH}_4$ .<sup>15</sup>

The separation factors for  $\text{CO}_2$  over  $\text{CH}_4$  based on the static adsorption capacities at temperatures of 273 and 298 K for various pressures up to 993 kPa are shown in Figure 7. At 273 K, the separation factors for all of the samples are quite similar, but the separation factors show a difference at 298 K. In general,  $\text{UiO-66-(OH)}_2$  presents the highest separation factors while  $\text{UiO-66-(OH)}_2\text{-NO}_2$  exhibits the lowest values. The  $\text{CO}_2/\text{CH}_4$  separation factors of the singly functionalized samples  $\text{UiO-66-(OH)}_2$  and  $\text{UiO-66-NO}_2$  are slightly higher than those of the binary-functionalized samples. This may be related to weaker functional group interconnection of the high mesopore volumes of  $\text{UiO-66-(OH)}_2$  and  $\text{UiO-66-NO}_2$ , which favors the adsorption of  $\text{CO}_2$  rather than  $\text{CH}_4$ , whereas the strong interconnection in the micropores of the materials such as  $\text{UiO-66-(OH)}_2\text{-NO}_2$  and  $\text{UiO-66-NO}_2\text{-(OH)}_2$  can enhance the  $\text{CH}_4$  uptake. In addition, adsorbate–surface interactions could be another reason for the low separation factors for  $\text{CO}_2$  over  $\text{CH}_4$  on the binary-functionalized samples.  $\text{UiO-66-(OH)}_2$  shows higher separation factors to separate  $\text{CO}_2$  from  $\text{CH}_4$ , especially at low pressures up to 100 kPa; the separation factors range from 4.9 at about 100 kPa to 5.8 at 60 kPa at 298 K.

The isosteric heats of adsorption ( $Q_{st}$ ) for  $\text{CO}_2$  and  $\text{CH}_4$  in Figures 8 and 9 were calculated from the isotherms measured at 273 and 298 K using the Clausius–Claperyron equation:

$$\Delta H = -R \left( \frac{T_2 T_1}{T_2 - T_1} \right) \ln \left( \frac{P_2}{P_1} \right)$$

where  $P_1$  and  $T_1$  are the lower temperature and pressure,  $P_2$  and  $T_2$  are the higher pressure and temperature, and  $R$  is the universal gas constant ( $8.314 \text{ J}\cdot\text{mol}^{-1}\cdot\text{K}^{-1}$ ). Table 2 provides the isosteric heats adsorption of  $\text{CH}_4$  and  $\text{CO}_2$  on the singly and binary-functionalized  $\text{UiO-66-(OH)}_2$  and  $\text{UiO-66-NO}_2$  MOFs as well as other MOFs.

As shown in Figure 8, the isosteric heats of  $\text{CO}_2$  adsorption at different  $\text{CO}_2$  coverages on singly functionalized  $\text{UiO-66-(OH)}_2$  and  $\text{UiO-66-NO}_2$  were found to be on average  $\sim 33$  and  $\sim 28 \text{ kJ/mol}$ , respectively. On binary-functionalized  $\text{UiO-66-(OH)}_2\text{-NO}_2$  and  $\text{UiO-66-NO}_2\text{-(OH)}_2$ , the values were  $\sim 29$  and  $\sim 30 \text{ kJ/mol}$ , respectively. The decrease in isosteric heat of adsorption with  $\text{CO}_2$  gas loading is due to the highly heterogeneous adsorbents with a wide distribution of gas–solid interaction energies.<sup>37</sup>  $\text{CO}_2$  as a quadrupolar gas has a strong interaction with polar functional groups. The greater coverage of  $\text{CO}_2$  on the solid surface prevents additional  $\text{CO}_2$  molecules from being adsorbed and thus decreases isosteric heat. The energetic values for  $\text{CO}_2$  adsorption are quite similar to those of  $\text{UiO-66}$  reported previously,<sup>22,25,38,39</sup> while they are lower than those of other adsorbents, including Ni-MOF-74 ( $\sim 42 \text{ kJ/mol}$ ),<sup>40</sup> bio-MOF-11 ( $\sim 45 \text{ kJ/mol}$ ),<sup>41</sup> Mg-MOF-74 ( $\sim 47 \text{ kJ/mol}$ ),<sup>40</sup> NaX ( $\sim 48 \text{ kJ/mol}$ ),<sup>42</sup> and zeolite 13X ( $\sim 45 \text{ kJ/mol}$ ).<sup>43</sup> In addition, the  $\text{CO}_2$  isosteric heats of adsorption of the MixMOF sample  $\text{UiO-66-(OH)}_2\text{-NO}_2$  were decreased after loading with the  $\text{BDC-NO}_2$  functional group and vice versa for the MixMOF  $\text{UiO-66-NO}_2\text{-(OH)}_2$ . This can be attributed to the different polarities of the functional groups ( $\text{BDC-(OH)}_2 > \text{BDC-NO}_2$ ) and pore volumes of the samples.<sup>12,22,44</sup>

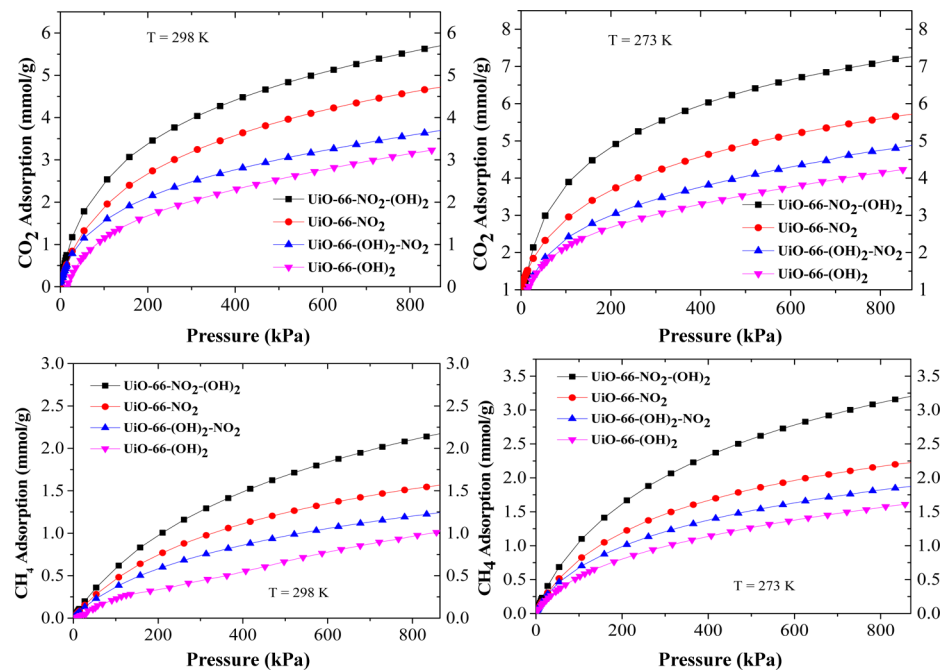


**Figure 6.**  $\text{CO}_2$  and  $\text{CH}_4$  adsorption isotherms for  $\text{UiO-66}$  samples at 298 and 273 K.

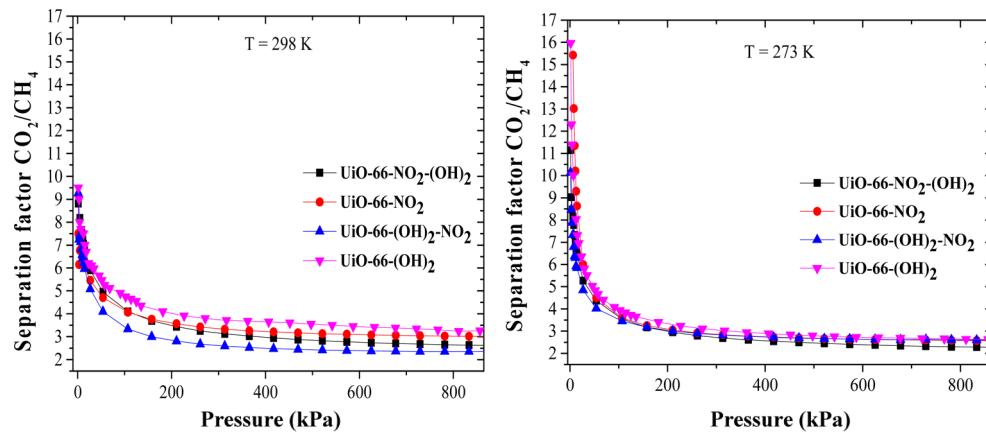


**Figure 7.** Separation factors for  $\text{CO}_2$  over  $\text{CH}_4$  for various  $\text{UiO-66}$  samples at 298 and 273 K.

**Table 2. Isosteric Heats of  $\text{CO}_2$  and  $\text{CH}_4$  Adsorption on Various MOFs**

MOF	$Q_{st}$ (kJ/mol)		refs
	$\text{CO}_2$	$\text{CH}_4$	
$\text{UiO-66-NO}_2$	29	22	25
$\text{UiO-66-NO}_2$	31	21	22
$\text{UiO-66-NO}_2$	30	—	38
$\text{UiO-66-NO}_2$	28	24	this work
$\text{UiO-66-NO}_2\text{-}(\text{OH})_2$	30	22	this work
$\text{UiO-66-(OH)}_2$	29	20	22
$\text{UiO-66-(OH)}_2$	30	—	39
$\text{UiO-66-(OH)}_2$	33	31	this work
$\text{UiO-66-(OH)}_2\text{-NO}_2$	29	27	this work
Ni-MOF-74	42	20	40, 46
bio-MOF-11	45	—	41
Mg-MOF-74	47	18	40, 47
PCN-14	—	30	40

Figure 9 indicates that the isosteric heats of  $\text{CH}_4$  adsorption on all of the samples increased with gas loading, which is due to cooperative interactions between adsorbed molecules and the nonheterogeneous adsorbents.<sup>25,37,45</sup>  $\text{CH}_4$  is a nonpolar gas, and its interactions with solid surfaces bearing polar functional groups are not strong. However, with increased loading of  $\text{CH}_4$ , more dispersion of  $\text{CH}_4$  on the polar surface will occur, resulting in increased isosteric heat. Meanwhile, the average values of the isosteric heats of  $\text{CH}_4$  adsorption at different  $\text{CH}_4$  coverages were also determined to be  $\sim 31$ ,  $\sim 24$ ,  $\sim 27$ , and  $\sim 22$  kJ/mol on  $\text{UiO-66-(OH)}_2$ ,  $\text{UiO-66-NO}_2$ ,  $\text{UiO-66-(OH)}_2\text{-NO}_2$ , and  $\text{UiO-66-NO}_2\text{-}(\text{OH})_2$ , respectively. The isosteric heats of  $\text{CH}_4$  adsorption on the MixMOFs samples  $\text{UiO-66-(OH)}_2\text{-NO}_2$  and  $\text{UiO-66-NO}_2\text{-}(\text{OH})_2$  were lower than those of the singly functionalized samples  $\text{UiO-66-(OH)}_2$  and  $\text{UiO-66-NO}_2$ , which can still be related to the lower strength of the dipole–dispersion and dispersion–dispersion interactions of  $\text{CH}_4$  with the solid surfaces.<sup>25,45</sup> Having more polar functional groups on the solid surface does not favor  $\text{CH}_4$  adsorption.

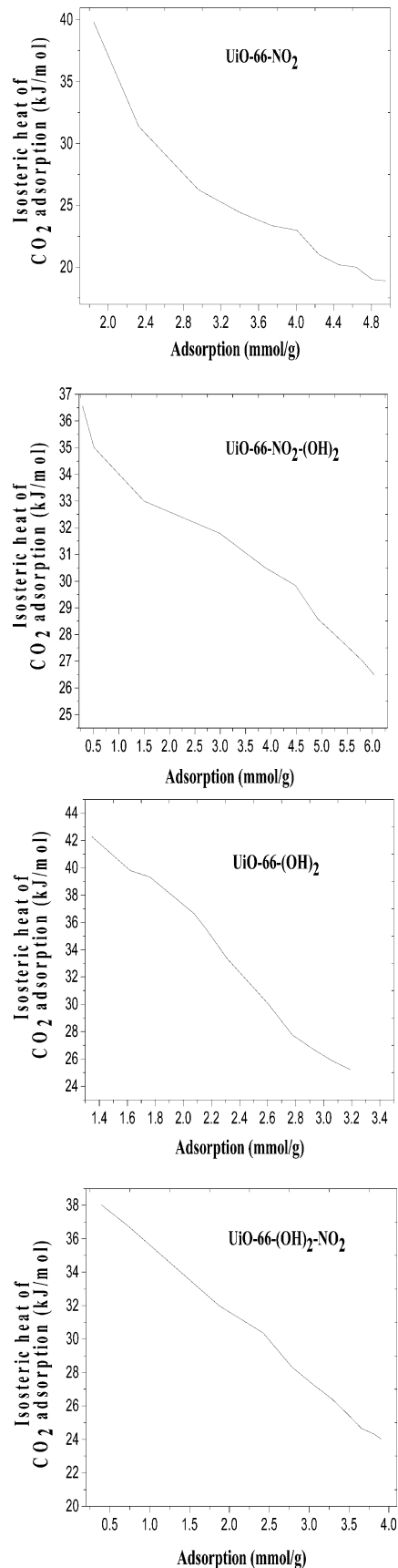


**Figure 8.** Variations in the isosteric heat of  $\text{CO}_2$  adsorption on  $\text{UiO-66-(OH)}_2$ ,  $\text{UiO-66-(OH)}_2\text{-NO}_2$ ,  $\text{UiO-66-NO}_2$ , and  $\text{UiO-66-NO}_2\text{-(OH)}_2$  samples at different adsorbed volumes.

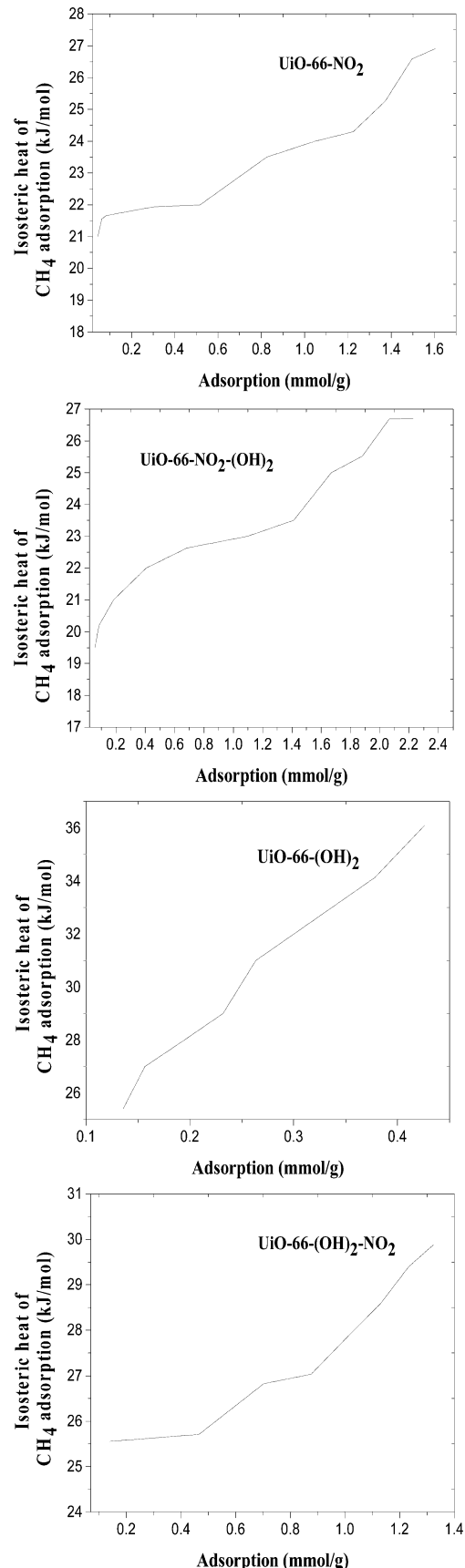


**Figure 9.** Variations in isosteric heat of  $\text{CH}_4$  adsorption for  $\text{UiO-66-(OH)}_2$ ,  $\text{UiO-66-(OH)}_2\text{-NO}_2$ ,  $\text{UiO-66-NO}_2$  and  $\text{UiO-66-NO}_2\text{-(OH)}_2$  samples at different adsorbed volumes.

## 4. CONCLUSIONS

Singly functionalized UiO-66-(OH)<sub>2</sub> and UiO-66-NO<sub>2</sub> and binary-functionalized UiO-66-(OH)<sub>2</sub>-NO<sub>2</sub> and UiO-66-NO<sub>2</sub>-(OH)<sub>2</sub> were synthesized and activated by methanol at mild temperatures. The effects of the hydroxyl and nitro groups on the UiO-66 structures and CO<sub>2</sub> and CH<sub>4</sub> adsorption were investigated. UiO-66-(OH)<sub>2</sub> has a lower BET surface area and CO<sub>2</sub> and CH<sub>4</sub> adsorption capacities than UiO-66-NO<sub>2</sub>. However, UiO-66-(OH)<sub>2</sub> has a higher efficiency in selective adsorption of CO<sub>2</sub> over CH<sub>4</sub>. Binary-functionalized UiO-66-(OH)<sub>2</sub>-NO<sub>2</sub> and UiO-66-NO<sub>2</sub>-(OH)<sub>2</sub> show higher uptakes of CO<sub>2</sub> and CH<sub>4</sub> than singly functionalized UiO-66.

## ■ AUTHOR INFORMATION

### Corresponding Author

\*E-mail: shaobin.wang@curtin.edu.au. Tel: +61 8 92663776. Fax: +61 8 92662681.

### Notes

The authors declare no competing financial interest.

## ■ ACKNOWLEDGMENTS

We thank Ms. Elaine Miller for SEM measurements. We also acknowledge the Ministry of Higher Education and Minister of Natural Resources/Kurdistan Regional Government-Iraq for a Ph.D. scholarship.

## ■ REFERENCES

- (1) Férey, G.; Mellot-Draznieks, C.; Serre, C.; Millange, F. Crystallized frameworks with giant pores: are there limits to the possible? *Acc. Chem. Res.* **2005**, *38*, 217–225.
- (2) Britt, D.; Tranchemontagne, D.; Yaghi, O. M. Metal-organic frameworks with high capacity and selectivity for harmful gases. *Proc. Natl. Acad. Sci. U. S. A.* **2008**, *105*, 11623–11627.
- (3) James, S. L. Metal-organic frameworks. *Chem. Soc. Rev.* **2003**, *32*, 276–288.
- (4) Seo, J. S.; Whang, D.; Lee, H.; Jun, S. I.; Oh, J.; Jeon, Y. J.; Kim, K. A homochiral metal-organic porous material for enantioselective separation and catalysis. *Nature* **2000**, *404*, 982–986.
- (5) Li, J.-R.; Kuppler, R. J.; Zhou, H.-C. Selective gas adsorption and separation in metal-organic frameworks. *Chem. Soc. Rev.* **2009**, *38*, 1477–1504.
- (6) Cui, Y.; Yue, Y.; Qian, G.; Chen, B. Luminescent functional metal-organic frameworks. *Chem. Rev.* **2012**, *112*, 1126–1162.
- (7) Cavka, J. H.; Grande, C. A.; Mondino, G.; Blom, R. High pressure adsorption of CO<sub>2</sub> and CH<sub>4</sub> on Zr-MOFs. *Ind. Eng. Chem. Res.* **2014**, *53*, 15500–15507.
- (8) Taylor-Pashow, K. M.; Rocca, J. D.; Xie, Z.; Tran, S.; Lin, W. Postsynthetic modifications of iron-carboxylate nanoscale metal-organic frameworks for imaging and drug delivery. *J. Am. Chem. Soc.* **2009**, *131*, 14261–14263.
- (9) Wei, J.; Liao, L.; Xiao, Y.; Zhang, P.; Shi, Y. Capture of carbon dioxide by amine-impregnated as-synthesized MCM-41. *J. Environ. Sci.* **2010**, *22*, 1558–1563.
- (10) Mishra, P.; Uppara, H. P.; Mandal, B.; Gumma, S. Adsorption and separation of carbon dioxide using MIL-53 (Al) metal-organic framework. *Ind. Eng. Chem. Res.* **2014**, *53*, 19747–19753.
- (11) Yazaydin, A. O.; Benin, A. I.; Faheem, S. A.; Jakubczak, P.; Low, J. J.; Willis, R. R.; Snurr, R. Q. Enhanced CO<sub>2</sub> adsorption in metal-organic frameworks via occupation of open-metal sites by coordinated water molecules. *Chem. Mater.* **2009**, *21*, 1425–1430.
- (12) Rada, Z. H.; Abid, H. R.; Shang, J.; He, Y.; Webley, P.; Liu, S.; Sun, H.; Wang, S. Effects of amino functionality on uptake of CO<sub>2</sub>, CH<sub>4</sub> and selectivity of CO<sub>2</sub>/CH<sub>4</sub> on titanium based MOFs. *Fuel* **2015**, *160*, 318–327.
- (13) Bae, Y.-S.; Farha, O. K.; Hupp, J. T.; Snurr, R. Q. Enhancement of CO<sub>2</sub>/N<sub>2</sub> selectivity in a metal-organic framework by cavity modification. *J. Mater. Chem.* **2009**, *19*, 2131–2134.
- (14) Bae, Y.-S.; Hauser, B. G.; Farha, O. K.; Hupp, J. T.; Snurr, R. Q. Enhancement of CO<sub>2</sub>/CH<sub>4</sub> selectivity in metal-organic frameworks containing lithium cations. *Microporous Mesoporous Mater.* **2011**, *141*, 231–235.
- (15) Bae, Y. S.; Snurr, R. Q. Development and evaluation of porous materials for carbon dioxide separation and capture. *Angew. Chem., Int. Ed.* **2011**, *50*, 11586–11596.
- (16) Dybtsev, D. N.; Chun, H.; Yoon, S. H.; Kim, D.; Kim, K. Microporous manganese formate: a simple metal-organic porous material with high framework stability and highly selective gas sorption properties. *J. Am. Chem. Soc.* **2004**, *126*, 32–33.
- (17) Bae, Y.-S.; Farha, O. K.; Spokoyny, A. M.; Mirkin, C. A.; Hupp, J. T.; Snurr, R. Q. Carborane-based metal-organic frameworks as highly selective sorbents for CO<sub>2</sub> over methane. *Chem. Commun.* **2008**, 4135–4137.
- (18) Wang, Z.; Cohen, S. M. Postsynthetic modification of metal-organic frameworks. *Chem. Soc. Rev.* **2009**, *38*, 1315–1329.
- (19) He, Y.; Li, B.; O'Keeffe, M.; Chen, B. Multifunctional metal-organic frameworks constructed from meta-benzenedicarboxylate units. *Chem. Soc. Rev.* **2014**, *43*, 5618–5656.
- (20) Couck, S.; Denayer, J. F.; Baron, G. V.; Rémy, T.; Gascon, J.; Kapteijn, F. An amine-functionalized MIL-53 metal-organic framework with large separation power for CO<sub>2</sub> and CH<sub>4</sub>. *J. Am. Chem. Soc.* **2009**, *131*, 6326–6327.
- (21) Zheng, B.; Yang, Z.; Bai, J.; Li, Y.; Li, S. High and selective CO<sub>2</sub> capture by two mesoporous acylamide-functionalized rht-type metal-organic frameworks. *Chem. Commun.* **2012**, *48*, 7025–7027.
- (22) Yang, Q.; Wiersum, A. D.; Llewellyn, P. L.; Guillerm, V.; Serre, C.; Maurin, G. Functionalizing porous zirconium terephthalate UiO-66 (Zr) for natural gas upgrading: a computational exploration. *Chem. Commun.* **2011**, *47*, 9603–9605.
- (23) Cavka, J. H.; Jakobsen, S.; Olsbye, U.; Guillou, N.; Lamberti, C.; Bordiga, S.; Lillerud, K. P. A new zirconium inorganic building brick forming metal organic frameworks with exceptional stability. *J. Am. Chem. Soc.* **2008**, *130*, 13850–13851.
- (24) Abid, H. R.; Shang, J.; Ang, H.-M.; Wang, S. Amino-functionalized Zr-MOF nanoparticles for adsorption of CO<sub>2</sub> and CH<sub>4</sub>. *Int. J. Smart Nano Mater.* **2013**, *4*, 72–82.
- (25) Cmarik, G. E.; Kim, M.; Cohen, S. M.; Walton, K. S. Tuning the adsorption properties of UIO-66 via ligand functionalization. *Langmuir* **2012**, *28*, 15606–15613.
- (26) Ethiraj, J.; Albanese, E.; Civalleri, B.; Vitillo, J. G.; Bonino, F.; Chavan, S.; Shearer, G. C.; Lillerud, K. P.; Bordiga, S. Carbon dioxide adsorption in amine-functionalized mixed-ligand metal-organic frameworks of UiO-66 topology. *ChemSusChem* **2014**, *7*, 3382–3388.
- (27) Kim, M.; Cahill, J. F.; Prather, K. A.; Cohen, S. M. Postsynthetic modification at orthogonal reactive sites on mixed, bifunctional metal-organic frameworks. *Chem. Commun.* **2011**, *47*, 7629–7631.
- (28) Chavan, S. M.; Shearer, G. C.; Svelle, S.; Olsbye, U.; Bonino, F.; Ethiraj, J.; Lillerud, K. P.; Bordiga, S. Synthesis and characterization of amine-functionalized mixed-ligand metal-organic frameworks of UiO-66 topology. *Inorg. Chem.* **2014**, *53*, 9509–9515.
- (29) Rada, Z. H.; Abid, H. R.; Sun, H.; Wang, S. Bifunctionalized metal organic frameworks, UIO-66-NO<sub>2</sub>-N (N=NH<sub>2</sub>, -(OH)<sub>2</sub>, -(COOH)<sub>2</sub>), for enhanced adsorption and selectivity of CO<sub>2</sub> and N<sub>2</sub>. *J. Chem. Eng. Data* **2015**, *60*, 2152–2161.
- (30) Braun, M. E.; Steffek, C. D.; Kim, J.; Rasmussen, P. G.; Yaghi, O. M. 1, 4-Benzenedicarboxylate derivatives as links in the design of paddle-wheel units and metal-organic frameworks. *Chem. Commun.* **2001**, 2532–2533.
- (31) Abid, H. R.; Pham, G. H.; Ang, H.-M.; Tade, M. O.; Wang, S. Adsorption of CH<sub>4</sub> and CO<sub>2</sub> on Zr-metal organic frameworks. *J. Colloid Interface Sci.* **2012**, *366*, 120–124.
- (32) Abid, H. R.; Tian, H.; Ang, H.-M.; Tade, M. O.; Buckley, C. E.; Wang, S. Nanosize Zr-metal organic framework (UiO-66) for

hydrogen and carbon dioxide storage. *Chem. Eng. J.* **2012**, *187*, 415–420.

(33) Li, B.; Wei, S.; Chen, L. Molecular simulation of CO<sub>2</sub>, N<sub>2</sub> and CH<sub>4</sub> adsorption and separation in ZIF-78 and ZIF-79. *Mol. Simul.* **2011**, *37*, 1131–1142.

(34) Banerjee, R.; Furukawa, H.; Britt, D.; Knobler, C.; O'Keeffe, M.; Yaghi, O. M. Control of pore size and functionality in isoreticular zeolitic imidazolate frameworks and their carbon dioxide selective capture properties. *J. Am. Chem. Soc.* **2009**, *131*, 3875–3877.

(35) Zhao, Y.; Wu, H.; Emge, T. J.; Gong, Q.; Nijem, N.; Chabal, Y. J.; Kong, L.; Langreth, D. C.; Liu, H.; Zeng, H.; Li, J. Enhancing gas adsorption and separation capacity through ligand functionalization of microporous metal–organic framework structures. *Chem. - Eur. J.* **2011**, *17*, 5101–5109.

(36) Llewellyn, P. L.; Bourrelly, S.; Serre, C.; Filinchuk, Y.; Férey, G. How hydration drastically improves adsorption selectivity for CO<sub>2</sub> over CH<sub>4</sub> in the flexible chromium terephthalate MIL-53. *Angew. Chem.* **2006**, *118*, 7915–7918.

(37) Dunne, J.; Mariwala, R.; Rao, M.; Sircar, S.; Gorte, R.; Myers, A. Calorimetric heats of adsorption and adsorption isotherms. I. O<sub>2</sub>, N<sub>2</sub>, Ar, CO<sub>2</sub>, CH<sub>4</sub>, C<sub>2</sub>H<sub>6</sub>, and SF<sub>6</sub> on silicalite. *Langmuir* **1996**, *12*, 5888–5895.

(38) Huang, Y.; Qin, W.; Li, Z.; Li, Y. Enhanced stability and CO<sub>2</sub> affinity of a UiO-66 type metal–organic framework decorated with dimethyl groups. *Dalton Trans.* **2012**, *41*, 9283–9285.

(39) Hu, Z.; Peng, Y.; Kang, Z.; Qian, Y.; Zhao, D. A modulated hydrothermal (MHT) approach for the facile synthesis of UiO-66-type MOFs. *Inorg. Chem.* **2015**, *54*, 4862–4868.

(40) Wu, H.; Zhou, W.; Yildirim, T. High-capacity methane storage in metal–organic frameworks M2 (dhtp): The important role of open metal sites. *J. Am. Chem. Soc.* **2009**, *131*, 4995–5000.

(41) An, J.; Geib, S. J.; Rosi, N. L. High and selective CO<sub>2</sub> uptake in a cobalt adeninate metal– organic framework exhibiting pyrimidine-and amino-decorated pores. *J. Am. Chem. Soc.* **2010**, *132*, 38–39.

(42) Shen, D.; Bülow, M.; Siperstein, F.; Engelhard, M.; Myers, A. L. Comparison of experimental techniques for measuring isosteric heat of adsorption. *Adsorption* **2000**, *6*, 275–286.

(43) Yang, Q.; Vaesen, S.; Ragon, F.; Wiersum, A. D.; Wu, D.; Lago, A.; Devic, T.; Martineau, C.; Taulelle, F.; Llewellyn, P. L.; Jobic, H.; Zhong, C.; Serre, C.; De Weireld, G.; Maurin, G. A water stable metal–organic framework with optimal features for CO<sub>2</sub> capture. *Angew. Chem.* **2013**, *125*, 10506–10510.

(44) Torrisi, A.; Bell, R. G.; Mellot-Draznieks, C. Functionalized MOFs for enhanced CO<sub>2</sub> capture. *Cryst. Growth Des.* **2010**, *10*, 2839–2841.

(45) Bourrelly, S.; Llewellyn, P. L.; Serre, C.; Millange, F.; Loiseau, T.; Férey, G. Different adsorption behaviors of methane and carbon dioxide in the isotropic nanoporous metal terephthalates MIL-53 and MIL-47. *J. Am. Chem. Soc.* **2005**, *127*, 13519–13521.

(46) Sumida, K.; Rogow, D. L.; Mason, J. A.; McDonald, T. M.; Bloch, E. D.; Herm, Z. R.; Bae, T.-H.; Long, J. R. Carbon dioxide capture in metal–organic frameworks. *Chem. Rev.* **2012**, *112*, 724–781.

(47) Mason, J. A.; Veenstra, M.; Long, J. R. Evaluating metal–organic frameworks for natural gas storage. *Chem. Sci.* **2014**, *5*, 32–51.